Trellis-Coded Quadrature-Phase-Shift Keying (QPSK) With Variable Overlapped Raised-Cosine Pulse Shaping

M. K. Simon,[1] P. Arabshahi,[1] and M. Srinivasan[1]

This article introduces the notion of uncoded, partially overlapped, staggered quadrature raised-cosine modulation (SQORC-P) as well as that of a trellis-coded form that is implemented as a specific embodiment of the recently introduced cross-correlated trellis-coded quadrature modulation (XTCQM). Consideration is given to the power spectral density (PSD) of the scheme over both linear and nonlinear channels as well as to its average bit-error probability (BEP) performance on an additive white Gaussian noise (AWGN) channel, the latter being characterized in terms of tight upper and lower bounds. It is shown that a continuously variable trade-off (as a function of the fractional overlap parameter, $0 \leq \alpha \leq 1$) between the rate of spectral roll-off and the amount of envelope fluctuation of the transmitted signal is achievable with a receiver average BEP performance that is virtually independent of the value of α and nominally equivalent to that of uncoded quadrature-phase-shift keying (QPSK).

I. Introduction

Quadrature overlapped raised-cosine (QORC) and staggered QORC (SQORC) modulations were introduced by Austin and Chang in 1981 [1] as schemes that offer a good combination of desirable spectral properties and error-probability performance. These authors analytically described the spectral behavior of these modulations on a linear additive white Gaussian noise (AWGN) channel and, in addition, presented computer simulation results for the same behavior over nonlinear channels characteristic of a traveling-wave tube (TWT) output. Specifically, it was shown that the power spectral density (PSD) of QORC (or SQORC) is equal to the product of that corresponding to minimum-shift keying (MSK) and that of quadrature-phase-shift keying (QPSK) or offset[2] QPSK (OQPSK) with identical transmitted bit rates. Thus, since the width of the main spectral lobe of MSK is 3/2 wider than that of QPSK, but its side lobes fall off two orders of magnitude faster (OQPSK varies as f^{-2} and MSK varies as f^{-4}), QORC and SQORC combine the advantageous properties of MSK and QPSK by having a first spectral null at $f = 1/2T_b$ (T_b is the bit duration in seconds) and an asymptotic spectral roll-off that varies as f^{-6}. Also, the QORC or SQORC waveform can be implemented with a transmitter similar to the quadrature form

---

[1] Communications Systems and Research Section.

[2] The terms "offset" and "staggered" are used interchangeably in the literature to indicate a modulation in which the in-phase (I) and quadrature-phase (Q) channels are delayed with respect to one another by one-half of a symbol interval. For QPSK modulation, the term "offset" is more common whereas, for QORC, the term "staggered" appears more often.

of modulator used to implement MSK, the difference being the shape of the transmitted pulse on the in-phase (I) and quadrature-phase (Q) channels.

In subsequent years, these schemes were studied further [2–6] both analytically and via simulation with regard to their spectral and error-probability performances over nonlinear band-limited channels. In all cases, the word "overlap" in the title of the acronym used to describe these modulations implied a 100 percent overlap of the two adjacent symbols with the one of interest. As such, QORC and SQORC are not constant-envelope modulations (unlike OQPSK, which is) and, in fact, their envelopes fluctuate as much as 3 dB. Nevertheless, despite the large envelope fluctuation, because of the staggering associated with SQORC, it was still shown in the previously cited references to be a desirable modulation on nonlinear channels from the standpoint of reducing the spectral side-lobe regrowth after bandpass filtering. What would be of interest would be a class of modulations that bridges the gap between OQPSK (constant envelope but slow spectral roll-off) and SQORC (maximum of 3-dB envelope fluctuation and rapid spectral roll-off), thereby allowing a continuous trade-off between these two conflicting properties.

By introducing the notion of partial overlap in the time domain (analogous to the notion of excess bandwidth associated with Nyquist signaling in the frequency domain), we shall describe, using a single fractional overlap parameter, α, a class of modulations referred to as uncoded, partially overlapped, staggered quadrature raised-cosine (SQORC-P) modulation, which at one extreme (no overlap) corresponds to OQPSK and at the other (full overlap) corresponds to SQORC. The parameter, α, therefore allows the system designer to continuously trade off between sharpness of spectral roll-off and degree of envelope fluctuation (which, as mentioned above, on a nonlinear channel is related to the amount of spectral side-lobe regrowth after bandpass filtering). We shall show that this parameterized form of SQORC has a PSD corresponding to the product of the PSD of OQPSK (with a channel—I or Q—rectangular symbol duration of $2T_b$) and the PSD of MSK (with a channel—I or Q—1/2-sinusoidal symbol duration of $2\alpha T_b$). Furthermore, the implementation of SQORC-P can be accomplished in the identical manner as that used to implement conventional SQORC. In particular, the pulse shape for SQORC-P can be obtained by passing a rectangular pulse of duration $2T_b$ through a filter with impulse response equal to that of an MSK pulse of duration $2\alpha T_b$.

Recently, a cross-correlated trellis-coded quadrature-modulation (XTCQM) scheme was introduced[3] that focuses on achieving a higher level of spectral containment than that inherent in the bandwidth efficiency of the traditional multilevel modulations, e.g., multiple phase-shift-keying (M-PSK) and quadrature amplitude modulation (QAM), associated with conventional trellis-coded techniques. The emphasis in XTCQM is on maintaining the quadrature identity of the transmitted signal, which is accomplished by applying an M-ary modulation (using different pulse shapes to distinguish among the members of the M-ary set) to each of the I and Q channels, the idea being to simplify the receiver structure (including the various synchronization subsystems). One special case of XTCQM considered in Footnote 3 occurs when there is no cross-correlation between the I and Q channels and either rectangular or purely sinusoidal waveshapes are used as the underlying transmitted waveforms on the I and Q channels in each symbol interval. With a simple rate 1/2, two-state encoder applied to the input I and Q symbol streams and an appropriate signal (waveshape)-mapping function applied to the encoder outputs, it was shown that the combined I–Q transmitted signal looks like a conventional (fully overlapped) SQORC in that it possesses the identical PSD but has the added advantage of increased power efficiency brought about by the inclusion of the two encoders.

In this article, we show that merely by changing one of the two waveforms assigned to the signal-mapping function, the same special case of XTCQM can be used to generate a transmitted waveform that spectrally resembles SQORC-P but again has the added power efficiency relative to the equivalent uncoded modulation. This class of modulations shall be referred to as trellis-coded OQPSK with variable

---

[3] M. K. Simon and T.-Y. Yan, "Cross-Correlated Trellis-Coded Quadrature Modulation (XTCQM)," provisional patent filed, CIT 2885, California Institute of Technology, Pasadena, California, October 5, 1998.

overlapped raised-cosine pulse shaping. While our primary interest is indeed in the trellis-coded case as per the above, we shall begin by first discussing the properties and means of generating an SQORC-P signal. Next we consider the PSD of this signal when transmitted over linear and nonlinear (hard-limited) channels. Following this, we shall present the optimum receiver for the trellis-coded case along with upper and lower bounds on its bit-error probability (BEP). Since the PSD and BEP are both expressed in terms of the overlap parameter, α, we shall be able to demonstrate the continuously variable trade-off (as a function of α) between the corresponding performances of the two extremes corresponding to a transmitted signal having rectangular pulse shaping ($\alpha = 0$) and one having fully overlapped raised-cosine pulse shaping ($\alpha = 1$) typical of OQPSK and SQORC modulations, respectively.

II. The Transmitter Model for Uncoded SQORC-P

Consider a binary source generating a random data sequence $\{d_n\}$ at rate $1/T_b$ b/s. At the transmitter, this data stream is split into even and odd data (symbol) sequences $\{a_n = d_{2n}\}$ and $\{b_n = d_{2n+1}\}$ assigned (arbitrarily) to the I and Q channels. As in all quadrature modulation schemes, each of these symbol sequences occurs at a rate of $1/2T_b = 1/T_s$, and the two are assumed to be synchronous with each other. The I and Q sequences (with rectangular pulses implied) are passed through identical I and Q pulse-shaping filters with impulse response

$$h\left(t\right) = \frac{\pi}{4\alpha T_b \sin\left(\frac{\pi}{2\alpha}\right)} \sin\left(\frac{\pi t}{2\alpha T_b}\right), \quad 0 \leq t \leq 2\alpha T_b \tag{1}$$

The response of this pulse-shaping filter to a unit amplitude rectangular pulse of duration $2T_b$ s is a pulse shape $p\left(t\right)$ (of duration $4T_b$) that has a raised-cosine roll-off at its edges, is flat in its middle, and has dead zones (zero value) at its beginning and end, i.e., (for convenience of notation, we define the pulse shape shifted to the left by $2T_b$ s so that it is symmetrical around $t = 0$—see Fig. 1)

$$p\left(t + 2T_b\right) = \begin{cases} 1, & 0 \leq |t| \leq (1 - \alpha)\,T_b \\ \cos^2 \dfrac{\pi\left(|t| - (1 - \alpha)\,T_b\right)}{4\alpha T_b}, & (1 - \alpha)\,T_b \leq |t| \leq (1 + \alpha)\,T_b \\ 0, & (1 + \alpha)\,T_b \leq |t| \leq 2T_b \end{cases} \tag{2}$$
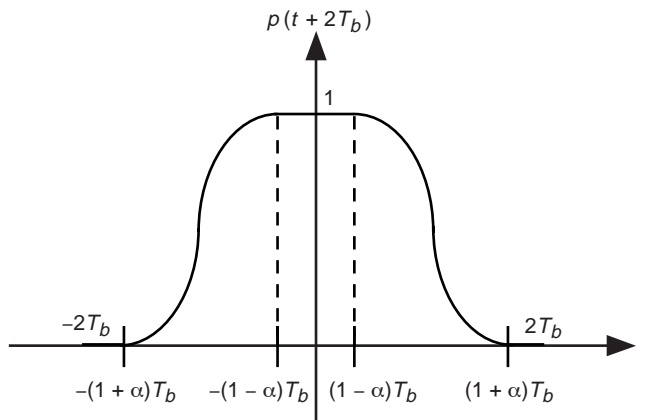
Fig. 1. The pulse shape for SQORC-P.

3

Thus, the result of passing the I and Q rectangular pulse data streams through the pulse-shaping filters is two streams of partially overlapped raised-cosine pulses. Figure 2 is an illustration of the partially overlapped data stream on the I channel for a typical data sequence and $\alpha = 0.5$ as an example. The partially overlapped I and Q data streams then are delayed with respect to one another by T_b s (as is the case for staggered-modulation schemes), modulated onto quadrature carriers, and then summed, producing the transmitted SQORC-P modulation

$$s(t) = A \sum_{n=-\infty}^{\infty} \{a_n p\,(t - 2nT_b) \cos\omega_c t + b_n p\,(t - (2n+1)\,T_b) \sin\omega_c t\} \tag{3}$$

where A is an amplitude scaling constant that is related to the average power, S, of $s\,(t)$ by
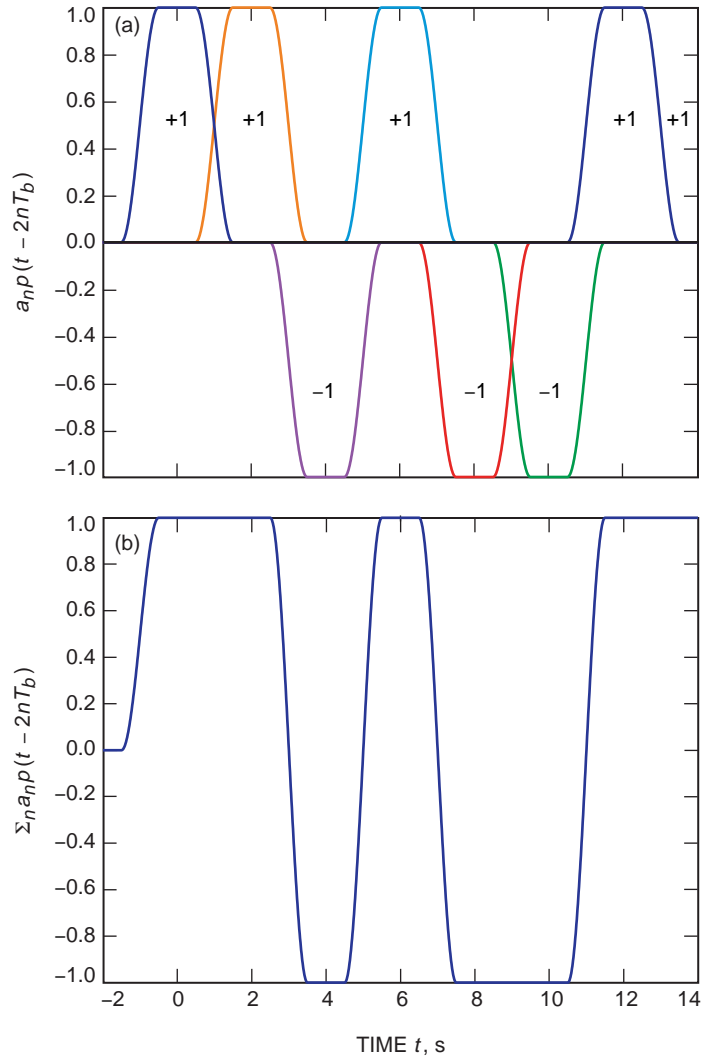
Fig. 2. An illustration of the partially overlapped data stream on the I channel: (a) single raised-cosine pulses for a +1,+1,–1,+1,–1,–1,+1,+1 pulse train and (b) the composite waveform ($T_b = 1$) – $\alpha = 0.5$.

4

$$A = \sqrt{\frac{S}{1 - \frac{\alpha}{4}}} \qquad (4)$$

A transmitter for generating the signal of Eq. (3) is illustrated in Fig. 3.

An alternate architecture for generating an SQORC-P signal is given in Fig. 4. Here, once again, the I and Q channel data streams, $\{a_n\}$ and $\{b_n\}$, at rate $1/2T_b$, which were originally obtained by splitting the data sequence $\{d_n\}$ at rate $1/T_b$ into its even and odd indices, now are each split once again into even and odd index subsequences (delayed by $2T_b$ with respect to each other) and occurring at rate $1/4T_b$. These subsequences then are applied to partially overlapped raised-cosine pulses of duration $4T_b$ [as typified by Eq. (2)] and summed back into a single data stream. Pulse-shape filtering here is thus effectively performed through a process of splitting, multiplication by $p(t)$, and recombining.

III. The PSD of SQORC-P Transmitted Over a Linear Channel

Since $p(t)$ is produced by the convolution of a rectangular $2T_b$ s pulse with the impulse response of Eq. (1), then the equivalent normalized (by $2T_b$) low-pass PSD of SQORC-P is easily seen to be (for simplicity, we have normalized A equal to unity)

$$\frac{S_m(f)}{2T_b} = \left| \frac{\sin 2\pi f T_b}{2\pi f T_b} \right|^2 \left| \frac{\cos 2\pi \alpha f T_b}{1 - 16\alpha^2 f^2 T_b^2} \right|^2 \qquad (5)$$
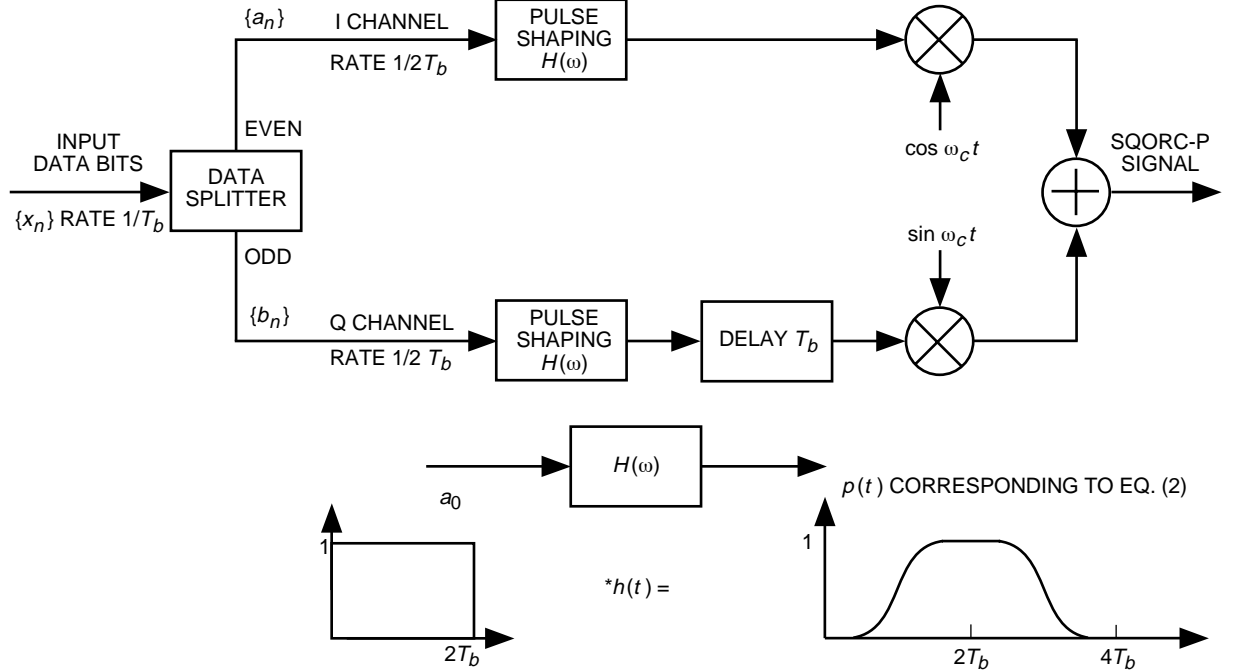
Fig. 3. Generating SQORC-P modulation via filtering.
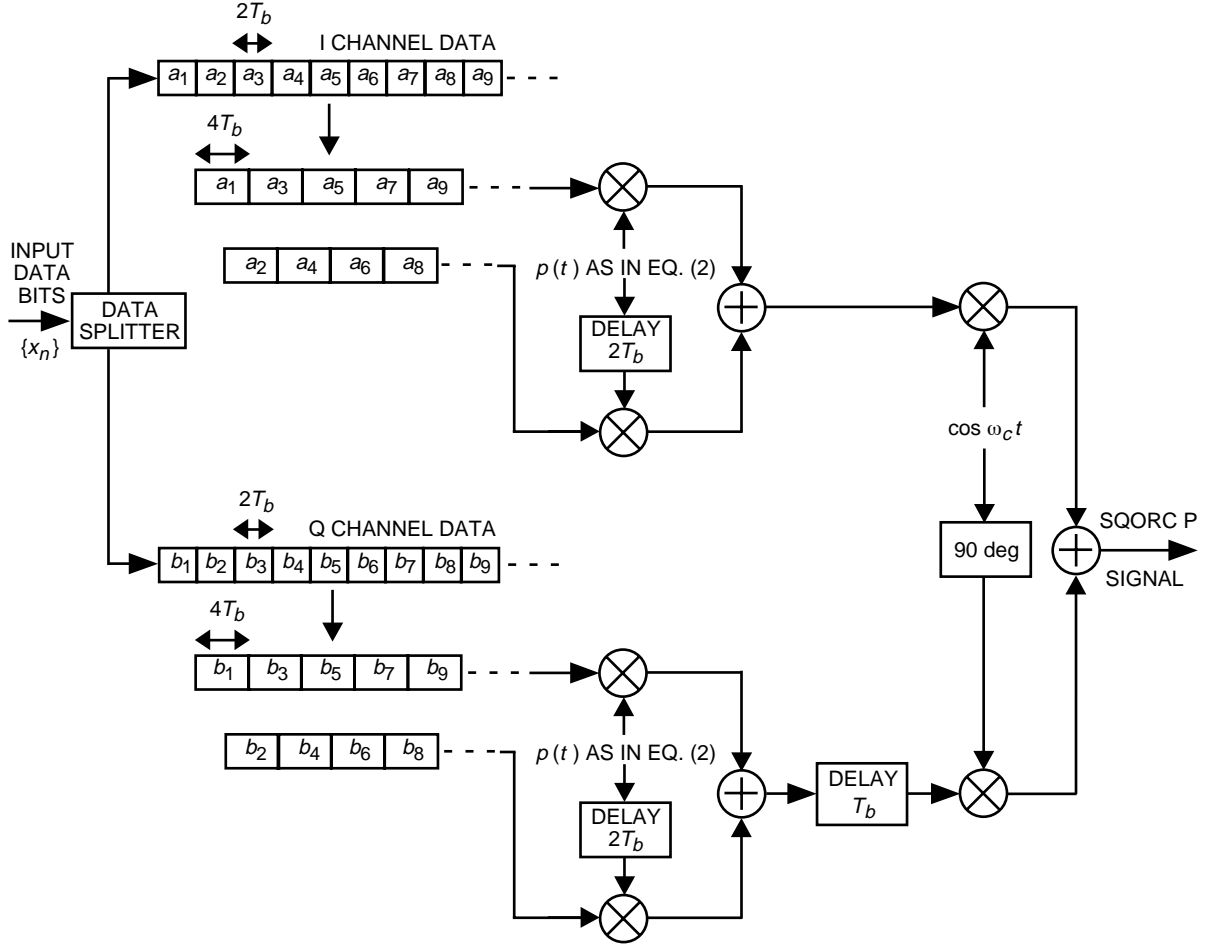
Fig. 4. An alternative architecture for generating SQORC-P modulation using multipliers.

where the first factor represents the PSD of OQPSK (with rectangular pulse shapes of duration $2T_b$ s) and the second factor represents the PSD of the I–Q form of MSK (with a half-sinusoidal pulse shape of duration $2\alpha T_b$ s). Note that, theoretically, for any $\alpha \neq 0$, the PSD of Eq. (4) rolls off asymptotically as f^{-6}, although the rate at which the PSD reaches this asymptote clearly increases as α increases. Figure 5 is an illustration of the PSD of Eq. (4) with α as a parameter varying from zero to one. We observe from this figure the corresponding gradual transition from the PSD of OQPSK to the PSD of SQORC.

IV. The PSD of SQORC-P Transmitted Over a Nonlinear Channel

Following steps analogous to those taken in [3] to determine the PSD of conventional SQORC over a nonlinear channel modeled as a hard limiter, e.g., at the output of a TWT operating in saturation, it can be shown that [3, Eq. (45)] also is applicable to SQORC-P provided that the appropriate pulse shapes are used to characterize the various terms in that expression. In particular, we have
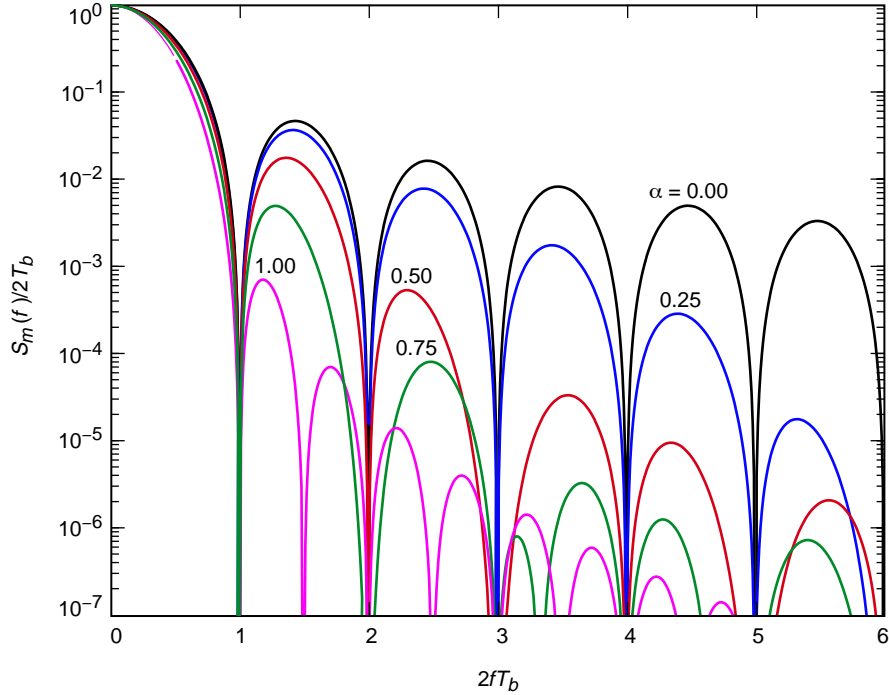
Fig. 5. The power spectral density of SQORC-P over a linear channel with α as a parameter.

$$\frac{S_m\left(f\right)}{2T_b} = \frac{3}{2}\sum_{k=1}^{4} R_k^2 + \frac{1}{2}\sum_{k=1}^{4} I_k^2$$

$$+ \frac{1}{4}\left[\left(\sum_{k=1}^{4} R_k\right)^2 + \left(\sum_{k=1}^{4} I_k\right)^2\right]\cos 8\pi fT_b - \frac{1}{2}\left(\sum_{k=1}^{4} R_k\right)\left(\sum_{k=1}^{4} I_k\right)\sin 8\pi fT_b$$

$$+ \left(R_1 + R_2 - R_3 - R_4\right)\left(\sum_{k=1}^{4} R_k \cos 4\pi fT_b - \sum_{k=1}^{4} I_k \sin 4\pi fT_b\right)$$

$$- R_1 R_3 - R_2 R_4 + I_1 I_3 + I_2 I_4 \tag{6}$$

where $R_k \triangleq \mathrm{Re}\left\{Y_k\right\}, I_k \triangleq \mathrm{Im}\left\{Y_k\right\}$, and the Y_k's are given as follows.

For $0 \le \alpha \le 1$,

$$Y_1 = \frac{1}{2\sqrt{2}}\left[\left(\frac{\sin 2\pi fT_b}{2\pi fT_b}\right) - j\left(\frac{\sin^2 \pi fT_b}{\pi fT_b}\right)\right] \tag{7}$$

$$Y_2 = \frac{1}{2\pi} \int_0^{\alpha\pi} \frac{\cos 2fT_bz}{\sqrt{1 + \sin^2\left(\frac{z}{2\alpha}\right)}} dz + \frac{1}{2\sqrt{2}} \left[\left(\frac{\sin 2\pi fT_b}{2\pi fT_b} \right) - \alpha \left(\frac{\sin 2\pi\alpha fT_b}{2\pi\alpha fT_b} \right) \right]$$

$$- j \left[\frac{1}{2\pi} \int_0^{\alpha\pi} \frac{\sin 2fT_bz}{\sqrt{1 + \sin^2\left(\frac{z}{2\alpha}\right)}} dz - \frac{1}{2\sqrt{2}} \left[\left(\frac{\cos 2\pi fT_b}{2\pi fT_b} \right) - \alpha \left(\frac{\cos 2\pi\alpha fT_b}{2\pi\alpha fT_b} \right) \right] \right] \qquad (8)$$

$$Y_3 = -\frac{(1-\alpha)}{2\sqrt{2}} \left(\frac{\sin 2\pi(1-\alpha)fT_b}{2\pi(1-\alpha)fT_b} \right) + \frac{1}{2\pi} \int_{(1-\alpha)\pi}^{\pi} \frac{\sin\left(\frac{z-\pi}{2\alpha}\right)\cos 2fT_bz}{\sqrt{1 + \sin^2\left(\frac{z-\pi}{2\alpha}\right)}} dz$$

$$- j \left[\frac{(1-\alpha)}{2\sqrt{2}} \left(\frac{\cos 2\pi(1-\alpha)fT_b - 1}{2\pi(1-\alpha)fT_b} \right) + \frac{1}{2\pi} \int_{(1-\alpha)\pi}^{\pi} \frac{\sin\left(\frac{z-\pi}{2\alpha}\right)\sin 2fT_bz}{\sqrt{1 + \sin^2\left(\frac{z-\pi}{2\alpha}\right)}} dz \right] \qquad (9)$$

For $0 \leq \alpha \leq 0.5$,

$$Y_4 = -\frac{1}{2\pi} \int_0^{\alpha\pi} \frac{\cos 2fT_bz}{\sqrt{1 + \sin^2\left(\frac{z}{2\alpha}\right)}} dz - \frac{1}{2\sqrt{2}} \left[(1-\alpha) \left(\frac{\sin 2\pi(1-\alpha)fT_b}{2\pi(1-\alpha)fT_b} \right) - \alpha \left(\frac{\sin 2\pi\alpha fT_b}{2\pi\alpha fT_b} \right) \right]$$

$$+ \frac{1}{2\pi} \int_{(1-\alpha)\pi}^{\pi} \frac{\sin\left(\frac{z-\pi}{2\alpha}\right)\cos 2fT_bz}{\sqrt{1 + \sin^2\left(\frac{z-\pi}{2\alpha}\right)}} dz$$

$$+ j \left[\frac{1}{2\pi} \int_0^{\alpha\pi} \frac{\sin 2fT_bz}{\sqrt{1 + \sin^2\left(\frac{z}{2\alpha}\right)}} dz - \frac{1}{2\sqrt{2}} \left[(1-\alpha) \left(\frac{\cos 2\pi(1-\alpha)fT_b}{2\pi(1-\alpha)fT_b} \right) - \alpha \left(\frac{\cos 2\pi\alpha fT_b}{2\pi\alpha fT_b} \right) \right] \right.$$

$$\left. - \frac{1}{2\pi} \int_{(1-\alpha)\pi}^{\pi} \frac{\sin\left(\frac{z-\pi}{2\alpha}\right)\sin 2fT_bz}{\sqrt{1 + \sin^2\left(\frac{z-\pi}{2\alpha}\right)}} dz \right] \qquad (10a)$$

whereas for $0.5 \leq \alpha \leq 1$,

$$Y_4 = -\frac{1}{2\pi}\int_0^{(1-\alpha)\pi}\frac{\cos 2fT_b z}{\sqrt{1+\sin^2\left(\frac{z}{2\alpha}\right)}}dz + \frac{1}{2\pi}\int_{(1-\alpha)\pi}^{\alpha\pi}\frac{\sin\left(\frac{z-\pi}{2\alpha}\right)\cos 2fT_b z}{\sqrt{\sin^2\left(\frac{z}{2\alpha}\right)+\sin^2\left(\frac{z-\pi}{2\alpha}\right)}}dz$$

$$+\frac{1}{2\pi}\int_{\alpha\pi}^{\pi}\frac{\sin\left(\frac{z-\pi}{2\alpha}\right)\cos 2fT_b z}{\sqrt{1+\sin^2\left(\frac{z-\pi}{2\alpha}\right)}}dz$$

$$+j\left[\frac{1}{2\pi}\int_0^{(1-\alpha)\pi}\frac{\sin 2fT_b z}{\sqrt{1+\sin^2\left(\frac{z}{2\alpha}\right)}}dz - \frac{1}{2\pi}\int_{(1-\alpha)\pi}^{\alpha\pi}\frac{\sin\left(\frac{z-\pi}{2\alpha}\right)\sin 2fT_b z}{\sqrt{\sin^2\left(\frac{z}{2\alpha}\right)+\sin^2\left(\frac{z-\pi}{2\alpha}\right)}}dz\right.$$

$$\left.-\frac{1}{2\pi}\int_{\alpha\pi}^{\pi}\frac{\sin\left(\frac{z-\pi}{2\alpha}\right)\sin 2fT_b z}{\sqrt{1+\sin^2\left(\frac{z-\pi}{2\alpha}\right)}}dz\right] \tag{10b}$$

Evaluating Eqs. (7), (8), (9), and (10b) at $\alpha = 1$ gives results identical to [3, Eq. 45)], corresponding to conventional SQORC. Also, at $\alpha = 0.5$, Eqs. (10a) and (10b) produce the identical result, as should be the case. Figure 6 is a plot of the PSD of Eq. (6) with overlap parameter α as a parameter. Simulation results for the fully overlapped case ($\alpha = 1$) also are indicated for analytical evaluations.

V. The Transmitter Model for Trellis-Coded OQPSK With Partially Overlapped Raised-Cosine Pulse Shaping

In the citation in Footnote 3, a new class of trellis-coded modulations called cross-correlated trellis-coded quadrature modulation (XTCQM) was introduced that combines the bandwidth efficiency of conventional modulation schemes with the power efficiency of error-correction coding, but in a way that maintains the desirable I–Q form of the transmitted signal. Although the generic form of this modulation allows for cross-correlation of the bits generated by the I and Q encoders, i.e., some of the I-encoded bits are used to define the Q-channel waveform and vice versa, specific embodiments also were considered that did not involve such cross-correlation. One of these embodiments with I and Q encoder outputs decoupled implements a signal with spectral properties identical to SQORC but that, from a detection viewpoint, has the properties of trellis-coded OQPSK with fully overlapped raised-cosine pulse shaping. A modulator representing this particular embodiment of XTCQM is illustrated in Fig. 7. Here, the I and Q data sequences, $\{a_n\}$ and $\{b_n\}$, respectively, once again are assumed to be time synchronous, each bit occurring during the interval $(2n-1)T_b \leq t \leq (2n+1)T_b$.[4] Letting $\{a_n'\}$ and $\{b_n'\}$ denote the (0,1) equivalents of the I and Q data sequences, i.e.,

---

[4] Since the choice for the specific time interval occupied by a single bit on the I or Q channel is arbitrary (provided that it is $T_s = 2T_b$ in duration), in this section we make this choice consistent with the notation introduced in the citation in Footnote 3.
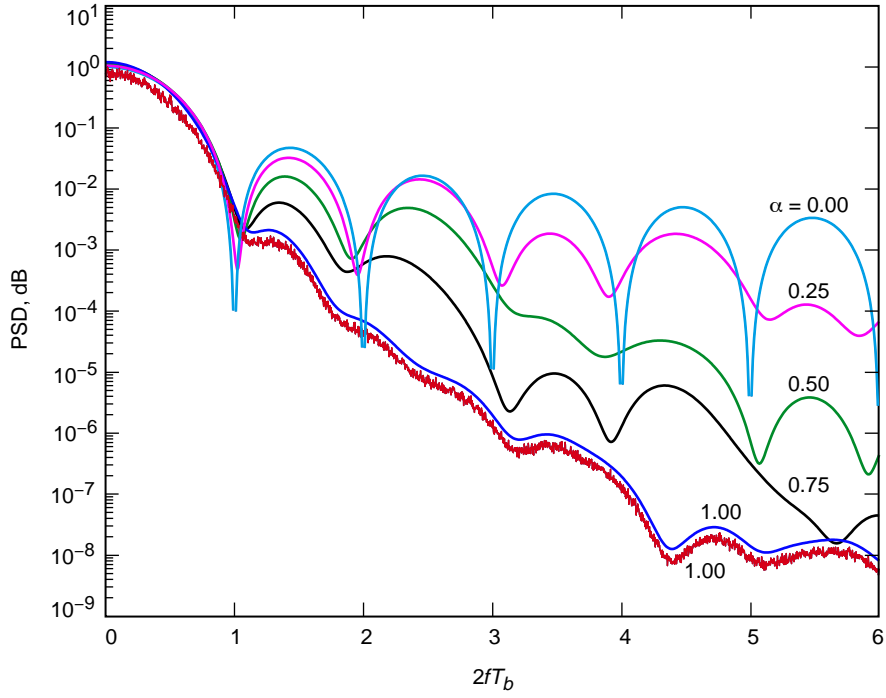
Fig. 6. The power spectral density of bandpass hard-limited SQORC-P (or trellis-coded OQPSK with partial overlapping). Simulated results (jagged line) are shown for $\alpha = 1$.
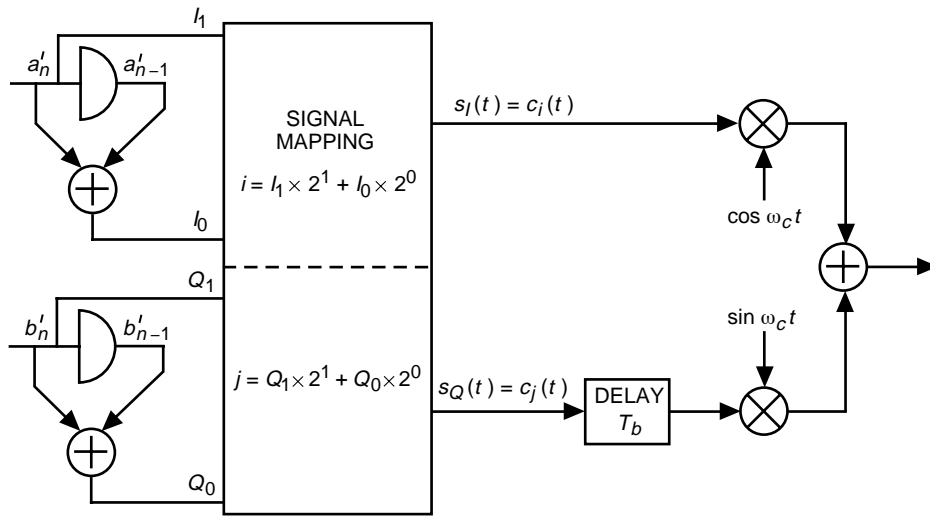
Fig. 7. The trellis-coded OQPSK embodiment of the XTCQM transmitter.

$$a'_n \triangleq \frac{1 - a_n}{2} \left.\vphantom{\begin{array}{c} \\ \\ \\ \\ \end{array}}\right\} \tag{11}$$

$$b'_n \triangleq \frac{1 - b_n}{2}$$

then encoding these sequences into the I and Q pairs, I_0, I_1 and Q_0, Q_1, in accordance with (see Fig. 7)

$$I_0 = a'_n \oplus a'_{n-1}, \quad I_1 = a'_n \left.\vphantom{\begin{array}{c} \\ \\ \\ \end{array}}\right\} \tag{12}$$

$$Q_0 = b'_n \oplus b'_{n-1}, \quad Q_1 = b'_n$$

and inputting these pairs to a binary-coded decimal (BCD) signal mapper that selects the pair of indices

$$i = I_0 \times 2^0 + I_1 \times 2^1 \left.\vphantom{\begin{array}{c} \\ \\ \\ \end{array}}\right\} \tag{13}$$

$$j = Q_0 \times 2^0 + Q_1 \times 2^1$$

the transmitted I and Q waveforms are chosen as

$$s_I(t) = c_i(t) \left.\vphantom{\begin{array}{c} \\ \\ \\ \end{array}}\right\} \tag{14}$$

$$s_Q(t) = c_j(t)$$

where the set $c_k(t)$; $k = 0, 1, 2, 3$ is defined by

$$c_0(t) = 1, \quad -T_b \le t \le T_b \left.\vphantom{\begin{array}{c} \\ \\ \\ \\ \\ \\ \\ \\ \\ \end{array}}\right\} \tag{15}$$

$$c_1(t) = \sin\left(\frac{\pi t}{2T_b}\right), \quad -T_b \le t \le T_b$$

$$c_2(t) = -c_0(t)$$

$$c_3(t) = -c_1(t)$$

That is, for each input pair of data bits a_n and b_n, a pair of indices i and j are selected that designate two of the four possible waveforms in Eq. (15) for transmission as the I and Q signals.

It is a simple matter to modify the XTCQM transmitter embodiment of Fig. 7 so that it generates a waveform whose spectral properties coincide with SQORC-P and whose detection has the characteristics of trellis-coded OQPSK with partially overlapped raised-cosine pulse shaping. In particular, it is straightforward to show that this can be accomplished by simply redefining $c_1(t)$ [and, therefore, its negative, $c_3(t) = -c_1(t)$] as

$$c_1(t) = \begin{cases} \sin\left(\dfrac{\pi t}{2\alpha T_b}\right), & 0 \le |t| \le \alpha T_b \\[2ex] 1, & \alpha T_b \le |t| \le T_b \end{cases} \tag{16}$$

That is, the form of the transmitter in Fig. 7 is still appropriate with merely a change in the signal set (two of the four) from which the I and Q signals are selected. Clearly in the limit of $\alpha = 1$, $c_1(t)$ of Eq. (16) reduces to its definition in Eq. (15), whereas in the limit of $\alpha = 0$, $c_1(t)$ of Eq. (16) becomes

$$c_1(t) = \text{sgn } t, \quad -T_b \le t \le T_b \tag{17}$$

which produces a transmitted waveform with the spectral properties of OQPSK and the detection characteristics of trellis-coded OQPSK (with the usual rectangular pulse shaping). Figure 8 illustrates the two unique waveforms, $c_0(t)$ of Eq. (15) and $c_1(t)$ of Eq. (16), for $\alpha = 0.25, 0.5, 0.75$, and 1.0, the latter corresponding to $c_1(t)$ of Eq. (15).

The I or Q channel of the transmitted modulation described above has a two-state trellis diagram, which is illustrated in Fig. 9. The dashed line indicates a transition caused by an input "0" to the shift register/XOR gate, and the solid line indicates a transition caused by an input "1." The branches are labeled with the output signal waveform ($s_I(t)$ or $s_Q(t)$ as appropriate) that results from the transition following the symbol mapping. The optimum receiver for such a trellis diagram and its performance will be discussed in the next section.
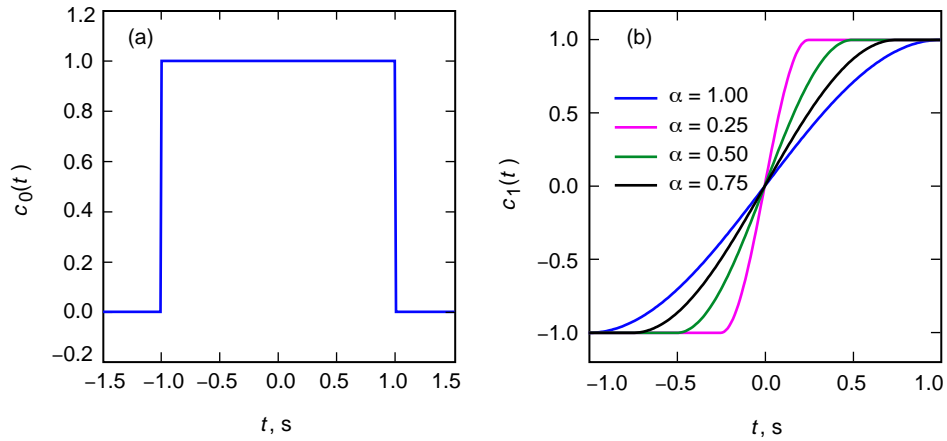
Fig. 8. Trellis-coded OQPSK with raised-cosine pulse-shaping full-symbol waveforms ($T_s = 2\,T_b = 2$): (a) $c_0(t) = -c_2(t)$ and (b) $c_1(t) = -c_3(t)$.
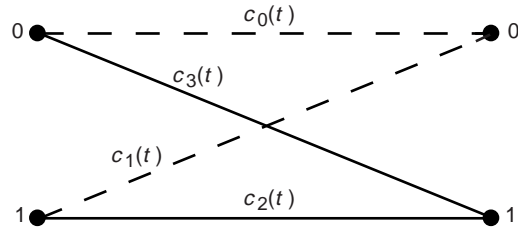
Fig. 9. The two-state trellis diagram for trellis-coded OQPSK with a raised-cosine pulse-shaping modulator.

Finally, the equivalence (in terms of the transmitted waveform) between the embodiment of the XTCQM modulator and the SQORC-P modulator discussed previously can be readily established. Consider the example of Fig. 2, where a sequence $\{a_n\} = \{+1, +1, -1, +1, -1, -1, +1, +1\}$ (or equivalently $\{a'_n\} = \{0, 0, 1, 0, 1, 1, 0, 0\}$) is transmitted in the I arm. From the trellis diagram of Fig. 9, the corresponding transmitted waveform sequence is $\{c_0(t), c_3(t), c_1(t), c_3(t), c_2(t), c_1(t), c_0(t), c_0(t)\}$,[5] which indeed is identical to the composite waveform in Fig. 2(b).

VI. The Optimum Reception and Bit-Error Probability Performance of Trellis-Coded OQPSK With Partially Overlapped Raised-Cosine Pulse Shaping

The optimum receiver for the waveform generated by the transmitter of Fig. 7 over a linear AWGN channel is discussed in the citation in Footnote 3 and illustrated here in Fig. 10. The input data waveforms are demodulated and then correlated with the two primary waveforms, $c_0(t)$ and $c_1(t)$, which then are passed through integrate-and-dump (I&D) filters (which, combined with the correlators, form matched filters). The structure of this receiver is the same for either fully or partially overlapped raised-cosine pulse shaping, the difference being the assignment of $c_1(t)$ to the correlators in accordance with Eq. (15) or Eq. (16), respectively. Four decision variables, Z_0, Z_1, Z_2, and Z_3, are formed, where $Z_2 = -Z_0$ and $Z_3 = -Z_1$ [since $c_2(t) = -c_0(t)$ and $c_3(t) = -c_1(t)$]. Due to the unequal energies of $c_0(t)$ and $c_1(t)$, namely, $E_0 = A^2$ and $E_1 = A^2(1 - \alpha/2)$, biases of $E_0/2$ and $E_1/2$ must be subtracted from the I&D outputs prior to forming the Z_i's. The decision variables then are fed to a Viterbi algorithm (VA) for final detection.
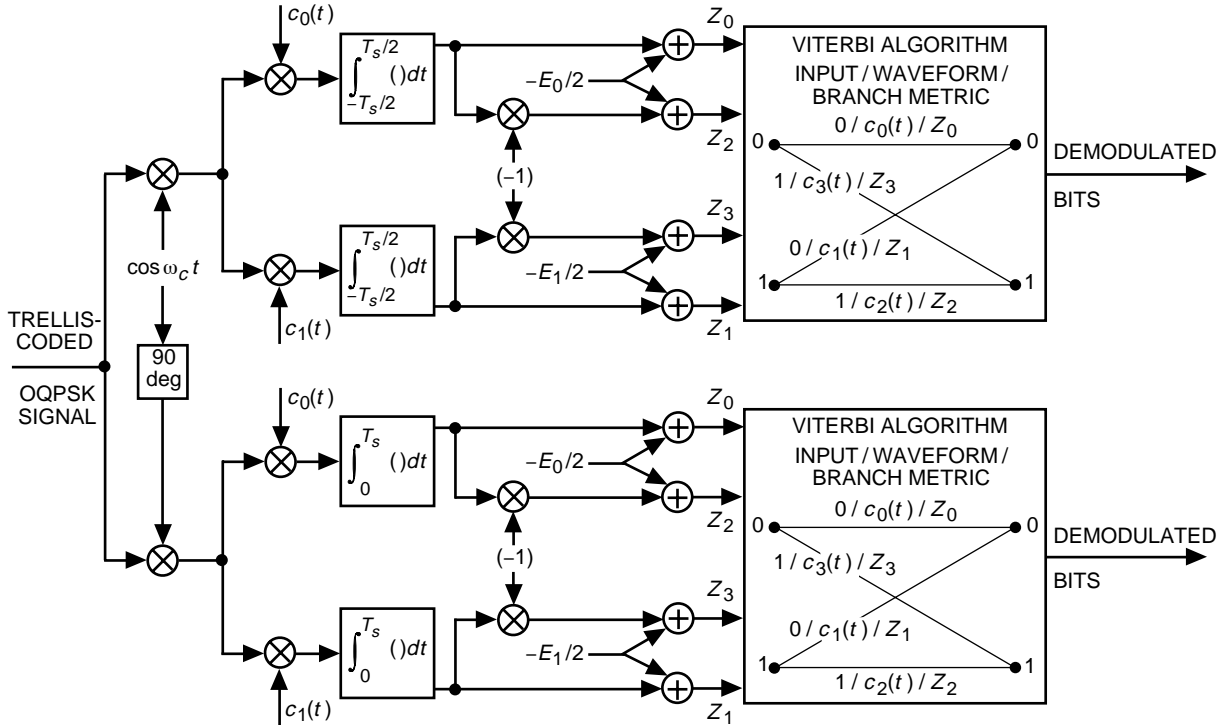
Fig. 10. The optimum receiver structure.

<hr />

[5] The first selected waveform, i.e., that corresponding to the interval $0 \le t \le 2T_b$, is discarded here since it depends on the initially random state of the shift register. For correspondence with Fig. 2(b), the initial state of the register would have been "1."

The procedure for computing the upper and lower bounds on the average BEP, $P_b(E)$, of the receiver in Fig. 10 is based on the transfer function bound approach outlined in [7]. (Derivations and examples appropriate to the case under consideration here are given on pp. 374–386 of [7] for trellis-coded QPSK.) In particular, the upper bound for the BEP over an AWGN channel is given by [7]

$$P_b \leq \frac{1}{m} Q\left(\sqrt{\frac{d_{\text{free}}^2 \bar{E}_b}{2N_0}}\right) \exp\left(\frac{d_{\text{free}}^2 \bar{E}_b}{4N_0}\right) \frac{\partial T(D, I)}{\partial I}\bigg|_{D=\exp(-\bar{E}_b/4N_0), I=1} \tag{18}$$

where d_{free}^2 is the square of the minimum free distance of the code, i.e., the minimum Euclidean distance between a pair of valid, distinct sequences of waveforms, $\bar{E}_b$ is the average energy per bit, N_0 is the single-sided PSD of the AWGN, and $T(D, I)$ is the transfer function associated with the state diagram derived from the trellis diagram. Since, for the case under consideration here, the squared minimum free distance is $d_{\text{free}}^2 = 4$ (independent of α), it is straightforward to show that

$$Q\left(\sqrt{\frac{2\bar{E}_b}{N_0}}\right) \leq P_b(E) \leq Q\left(\sqrt{\frac{2\bar{E}_b}{N_0}}\right) \frac{4}{\left[2 - \exp\left(-\frac{(1-[\alpha/2])}{(1-[\alpha/4])}\frac{\bar{E}_b}{N_0}\right) - \exp\left(-\frac{1}{(1-[\alpha/4])}\frac{\bar{E}_b}{N_0}\right)\right]^2} \tag{19}$$

where the lower bound is obtained from the single minimum distance path that diverges and remerges with the "0" state after two transitions, which corresponds to a single bit error.

For fully overlapped raised-cosine pulse shaping ($\alpha = 1$), the upper and lower bounds of (19) become

$$Q\left(\sqrt{\frac{2\bar{E}_b}{N_0}}\right) \leq P_b(E) \leq Q\left(\sqrt{\frac{2\bar{E}_b}{N_0}}\right) \frac{4}{\left[2 - \exp\left(-\frac{2\bar{E}_b}{3N_0}\right) - \exp\left(-\frac{4\bar{E}_b}{3N_0}\right)\right]^2} \tag{20}$$

whereas for rectangular pulse shaping ($\alpha = 0$), the upper and lower bounds of (19) become

$$Q\left(\sqrt{\frac{2\bar{E}_b}{N_0}}\right) \leq P_b(E) \leq Q\left(\sqrt{\frac{2\bar{E}_b}{N_0}}\right) \frac{1}{\left[1 - \exp\left(-\frac{\bar{E}_b}{N_0}\right)\right]^2} \tag{21}$$

Asymptotically ($\bar{E}_b/N_0$ large), the upper and lower bounds of (19) converge toward equality, which indicates that, for any $0 \leq \alpha \leq 1$, the BEP approaches that of uncoded QPSK (or OQPSK), namely, $P_b(E) = Q\left(\sqrt{2\bar{E}_b/N_0}\right)$. For the fully overlapped case, plots of $P_b(E)$ obtained from simulation of the receiver in Fig. 10 and the bounds of (20) are illustrated in Fig. 11. It is observed that over a wide range of $\bar{E}_b/N_0$, the lower bound is an excellent approximation of the true performance obtained via computer simulation. Since the lower bound is independent of α, and since the upper bound of (21) (corresponding to $\alpha = 0$) is even tighter than the bounds of (20) (corresponding to $\alpha = 1$), one would anticipate the same degree of tightness for the fit of the lower bound to simulated results here for any partially overlapped case.
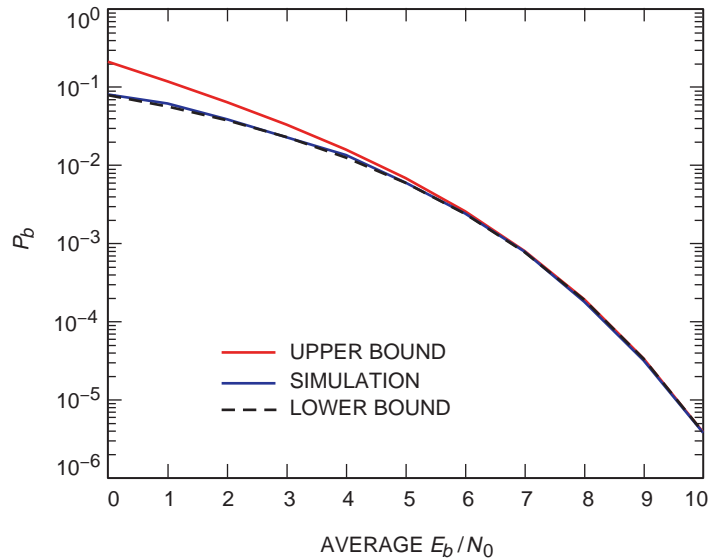
Fig. 11. The simulated BEP and the bounds on the BEP for trellis-coded OQPSK with fully overlapped ($\alpha = 1$) raised-cosine pulse shaping.

VII. Conclusion

In conclusion, trellis-coded OQPSK with partially overlapped raised-cosine pulse shaping offers the system designer the flexibility of a continuously variable trade-off (as α varies between 0 and 1) between the rate of spectral roll-off and the amount of envelope fluctuation of the transmitted signal with a receiver BEP performance that is virtually independent of the value of α and nominally equivalent to that of uncoded QPSK. Furthermore, it should be noted that, if one desires to surround the above trellis-coded modulation scheme with an additional error-correction encoder/decoder, then a soft output Viterbi algorithm (SOVA) [8] would replace the traditional hard decision VA output in Fig. 10.

References

[1] M. C. Austin and M. U. Chang, "Quadrature Overlapped Raised-Cosine Modulation," *Proc. Int. Conf. Commun.*, pp. 26.7.1–26.7.5, 1980; also *IEEE Trans. Commun.*, vol. COM-29, no. 3, pp. 237–249, March 1981.

[2] D. Divsalar and M. K. Simon, "Performance of Quadrature Overlapped Raised-Cosine Modulation Over Nonlinear Satellite Channels," *Proc. Int. Conf. Commun.*, Denver, Colorado, pp. 2.3.1–2.3.7, 1981.

[3] M. K. Simon, J. K. Omura, and D. Divsalar, "Performance of Staggered Quadrature Modulations Over Nonlinear Satellite Channels With Uplink Noise and Intersymbol Interference," *GLOBECOM Conf. Record*, Miami, Florida, pp. 190–197, 1982.

[4] D. Divsalar and M. K. Simon, "The Power Spectral Density of Digital Modulations Transmitted Over Nonlinear Channels," *IEEE Trans. Commun.*, vol. COM-30, no. 1, pp. 142–151, January 1982.

[5] X.-H. Chen and J. Oksman, "A Quasi-Constant Envelope Quadrature Over-lapped Modulation and Its Performance Over Nonlinear Band Limited Satellite Channels," *Int. Journ. Satellite Comm.*, vol. 14, pp. 351–359, 1996.

[6] X.-H. Chen and S.-Y. Wong, "Four Novel Quadrature Overlapping Modulations and Their Spectral Efficiency Analysis Over Band-Limited Non-Linear Channels," *Int. Journ. Satellite Comm.*, vol. 15, pp. 117–127, 1997.

[7] S. B. Wicker, *Error Control Systems for Digital Communication and Storage*, Englewood Cliffs, New Jersey: Prentice-Hall, Inc., 1995.

[8] J. Hagenauer and P. Hoeher, "A Viterbi Algorithm With Soft-Decision Outputs and Its Applications," *Proc. Globecom '89*, Dallas, Texas, pp. 1680–1686, November 1989.